Synsint Research Group

Available online at www.synsint.com

Synthesis and Sintering

ISSN 2564-0186 (Print), **ISSN** 2564-0194 (Online)

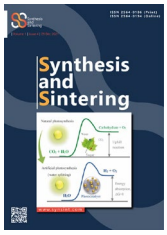

Research article

Challenges toward applying UHTC-based composite coating on graphite substrate by spark plasma sintering

Mehran Jaberi Zamharir, Mohammad Zakeri *, Mansour Razavi

Ceramics Department, Materials and Energy Research Center, Karaj, Iran

A B S T R A C T

In this study, the UHTC-based composite layers were applied on the graphite substrates using the SPS method to protect them against ablation. The protective layers had some defects and problems such as crack, fracture, separation, melting, and weak adhesion to the substrate. Several factors such as the thickness of the composite layer, the number of protective layers, the SPS conditions (temperature, applied pressure, soaking time and mold), the chemical composition of the layers, the type of the substrate and the mismatch between the thermal expansion coefficients of the substrate and the applied layer(s) affected the quality and connection of the protective layer to the graphite substrate. The amount of additive materials influenced the melting phenomenon in the composite layer; for example, further $MoSi_2$ in the layer led to more melting. The mismatch between the thermal expansion coefficients of the graphite substrate and the composite layer caused stresses during the cooling step, which resulted in cracks in the applied layer. Hence, proximity in the thermal expansion coefficients seems to be necessary for the formation of an acceptable adhesion between the layer and the substrate.

KEYWORDS

Carbon materials
Spark plasma sintering
Ultrahigh temperature ceramics
Protective layer
Thermal expansion coefficient

OPEN ACCESS

1. Introduction

Carbon materials and carbon-carbon composites are important materials in various industries like supersonic spacecraft, furnace elements, turbine blades, rocket nozzles, and space shuttle noses. These materials are promising candidates for high temperature usages where high strength and resistance to wear are demanded [1–6]. Carbon materials have gained researcher's attention because of their ability to withstand temperatures above 2500 °C without cooling fluids, high elastic modulus, good resistance to abrasion and fatigue, good machinability, low density, and high tensile strength at temperatures above 1200 °C [7–10]. However, some limitations of these components are severe oxidation at temperatures above 400 °C in oxidizing atmosphere, as well as weight loss and properties degradation at high temperatures. Therefore, it is necessary to use a coating to prevent the oxidation of carbon substrates at > 400 °C [11–14].

Ceramic coatings are mainly used to hinder the oxidation of carbonaceous materials [15–17]. Among ceramic materials, ultrahigh temperature ceramics (UHTCs) are utilized as coatings on the graphite, owing to their unique properties such as high melting temperature (above 3000 °C), excellent resistance to oxidation, and unique mechanical properties [18–20]. As a member of UHTCs, ZrB_2 is an appropriate choice for use in high temperature thermomechanical applications (> 2000 °C) [21–23]. Applying UHTCs coating on carbon-carbon composites to inhibit oxidation can be an acceptable approach to design the heat protection systems if it has followings [24]:

-Stability and integration to provide erosion resistance and limit evaporation.

-Ability to stop oxygen penetration into the substrate.

-Compatibility for resistance against lamination due to mismatch between the thermal expansion coefficients.

-Simple manufacturability and reproducibility.

* Corresponding author. *E-mail address:* m.zakeri@merc.ac.ir (M. Zakeri)

Received 20 September 2021; Received in revised form 20 December 2021; Accepted 20 December 2021.

https://doi.org/10.53063/synsint.2021.1452

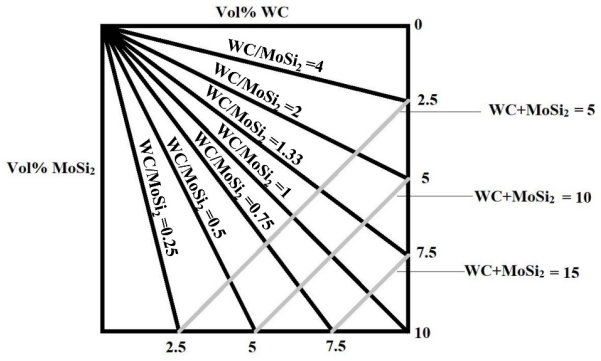

Fig. 1. Schematic of the compositional range of raw materials used for the outer composite layer.

There are several techniques to create coatings with fine microstructure such as spray deposition, electroplating, electron beam irradiation, slurry coating, pack cementation, and chemical vapor deposition. Each method has special advantages to control the thickness of the coating and the composition of the material [25–29]. To create a reliable UHTC coating and to optimize the penetration and adhesion of the carbon-carbon composite, understanding of the physical and chemical properties of the coating materials is [24, 30].

Various methods can be used to create UHTC coatings. Among them, spark plasma sintering (SPS) is a modern effective method due to the proper connection of coating materials with the substrate, the ability to control the thickness of the coating, the high durability of coating, and the desirable thermomechanical properties. Such coatings with high density and good thickness can increase corrosion and abrasion resistance, improve toughness and prevent graphite oxidation [31–35].

Many efforts have been done to increase the oxidation resistance of diborides. These studies showed that the addition of SiC to ZrB_2 greatly increases oxidation resistance at high temperatures [36–43]. Thermodynamic calculations of the oxidation of ZrB_2–SiC composites showed that the formation of a SiC-rich layer, a Zr-rich oxidized layer and a SiC-depleted ZrB_2 layer due to active oxidation of SiC decreased the oxidation rate [44]. In order to improve the oxidation resistance of carbon-carbon composites, a two-layer coating including ZrB_2 and SiC was applied. First, slurries containing ZrB_2 and SiC powders were prepared separately. Then, carbon-carbon composite samples were coated by squeeze infiltration in vacuum and heat-treated in argon atmosphere. The results showed that continuous multilayer coatings, including both SiC and ZrB_2 phases, are required for the protection of the carbon/carbon substrate [45].

In another study, after surface preparation of carbon-carbon composites, SiC coating was applied by low pressure chemical vapor deposition (LPCVD) at 1200 °C. Then, HfC-based coatings were deposited on SiC-coated samples at 1200 °C under atmospheric pressure. It should be noted that the precursor of the SiC coating was CH_3SiCl_3 and the precursors of the HfC coating were C_3H_6 and $HfCl_2$ [46].

Pack cementation method at 2100-1900 °C for 2 h was used to prepare ZrB_2–SiC coating on carbon/carbon composites in order to improve the erosion resistance. To increase the penetration rate, ZrB_2, Si, graphite and Al_2O_3 were chosen as the initial materials of the coating. During the pack cementation process, Si can react with the carbon/carbon composite to form SiC. Then, ZrB_2–SiC coating can be formed on the surface of carbon/carbon composites. Microstructural observations showed some microcracks on the surface of the coating due to the mismatch of thermal expansion coefficients between the coating and the carbon/carbon composite. The composite coating was dense without any infiltrative cracks or pores [47]. A multi-phase SiC–Si–ZrB_2 ceramic coating was applied on the surface of the SiC-coated carbon-carbon composite by powder pack cementation process. SiC bonding layer was formed on the surface of carbon-carbon composites using Si, C and Al_2O_3 powders at 1700-2000 °C for 2 h in argon atmosphere. Outer SiC–Si–ZrB_2 coating was applied on the surface of SiC-coated carbon-carbon composites at 1900-2200 °C for 2 h in an argon atmosphere using Si, B_2O_3, graphite and ZrB_2. The coating surface was dense and included microcracks that could be caused by rapid cooling to room temperature. The thickness of the coating was approximately 120 µm without any cracks or pores. In addition, there were no cracks or gaps between the inner SiC and the outer SiC–Si–ZrB_2 coatings, indicating a suitable bonding [48].

Table 1. Specifications of graphite substrate: type SB-1 (made in China).

Property	Value	Unit
Density	1.74	g/cm^3
Porosity	16	%
Bending strength	40	MPa
Compressive strength	85	MPa
Thermal conductivity	120	W/mK
Thermal expansion coefficient	4.6×10^{-6}	°C^{-1}
Elastic modulus	11	GPa
Carbon content	~94	%

Table 2. Specifications of graphite substrate: type TC-90 (made in Japan).

Property	Value	Unit
Density	1.80	g/cm^3
Hardness	80	Shore D
Mean particle size	5	µm
Specific resistance	15	µΩm
Bending strength	68	MPa
Tensile strength	50	MPa
Compressive strength	140	MPa
Elastic modulus	12	GPa
Thermal expansion coefficient	5×10^{-6}	°C^{-1}
Thermal conductivity	110	W/mK
Volatile substances (ash)	200	ppm

Table 3. Specifications of raw material powders used in protective layers.

Material	Particle size (μm)	Purity (%)	Supplier
ZrB_2	1–3	99.9	Hongwu International Group Ltd.
SiC	1–10	99.0	Hongwu International Group Ltd.
$MoSi_2$	3–10	99.5	Hongwu International Group Ltd.
WC	5–15	99.0	Almaseh Saz Co.
Si	< 12	99.0	Almaseh Saz Co.

A dense, well-bonded and crack-free ZrB_2–SiC–WC composite layer was applied on graphite substrate by SPS process at 1900 °C for 5 min. Microstructural observations displayed three regions in the cross-section of the coating: the upper ZrB_2–SiC–WC coating, the substrate/coating interface and the diffusion bond. No crack in the coating/substrate interface was seen in the ZrB_2–SiC–WC coating [31]. In this research, the protective layers of ultrahigh temperature ceramics are applied on the graphite substrates by the SPS route to increase their resistance against oxidation and ablation. Challenges, problems and defects in this methodology are identified and discussed to help researchers to overcome potential limitations.

2. Experimental procedure

2.1. Materials and methods

The graphite substrates with a diameter of 30 mm and a thickness of 5 mm were cut from graphite blocks of two different materials. The characteristics of the Chinese (SB-1) and Japanese (TC-90) graphite substrates are given in Tables 1 and 2, respectively. Sandpaper No. 400 was used to prepare the surface of the graphite substrates in order to create a uniform surface. The graphite substrates were then cleaned by ethanol using an ultrasonic device and finally dried in an oven at 100 °C for 2 h.

The specifications of the raw materials used in the composite protective layers are given in Table 3. Based on the design of experiments (Fig. 1), the raw material powders were weighed to prepare the composite mixtures. After that, the powders were ultrasonically mixed for 30 min in ethanol. Then, the obtained slurries were more mixed on a magnetic hot plate at 200 ºC with a rate of 300 rpm. The prepared powder mixtures were completely dried in an oven at 100 ºC for 24 h. Finally, the dried mixtures were passed through a 100-mesh sieve to minimize agglomeration.

Table 4. Chemical compositions of the outer composite layers chosen for the first methodology.

Sample code	Composition (vol%)			
	$MoSi_2$	WC	SiC	ZrB_2
Z-1	75	25	0	0
Z-2	71.25	23.75	2.5	2.5
Z-3	67.5	22.5	5	5
Z-4	63.75	21.25	7.5	7.5

The graphite mold used in this research has a diameter of 60 mm containing a hole with a diameter of 30 mm. The as-prepared powder mixtures were loaded on the graphite substrate embedded into the graphite mold, respectively. Then, the mold was placed inside the SPS furnace under vacuum conditions.

2.2. First methodology: double protective layers

In the first methodology, double protective layers were applied on the graphite substrates (type SB-1), as schematically shown in Fig. 2. The chemical composition of the intermediate layer was SiC-30 vol% Si. The volume ratio of ZrB_2/SiC in all outer composite layers was 3. The composition range of raw materials in the outer composite layer was considered based on the main diameter in Fig. 1 ($WC/MoSi_2$=1). Hence, five points were selected as the powder chemical compositions of the outer composite layers (Table 4).

To investigate the effect of Si addition in the composition of the outer layer as well as the role of the thickness of the intermediate layer (or its exclusion) on the connection and the quality of the protective layer, a new series of experiments was designed and performed as described in Table 5. Table 6 shows the sintering conditions applied to all samples made with the first methodology.

2.3. Second methodology: single protective layers

In this methodology, single protective layers were applied on the graphite substrates (type TC-90), as schematically displayed in Fig. 3. The volume ratio of ZrB_2/SiC+Si in the composite layer was considered approximately 2.33. The composition range of the raw materials was also selected based on the main diameter in Fig. 1 ($WC/MoSi_2$ = 1). The compositions of the chosen powder mixtures are presented in Table 7.

Table 5. Specifications of the protective layers for another series of samples applied to the type SB-1 graphite substrates.

Sample code	Outer layer				Intermediate layer		
	Composition (vol%)			Thickness (μm)	Composition (vol%)		Thickness (μm)
	Si	SiC	ZrB_2		Si	SiC	
T-1	15	15	70	700	50	50	300
T-2	-	30	70	700	50	50	200
T-3	15	15	70	700	-	-	-

Table 6. The SPS conditions for applying the UHTC-based layers on the type SB-1 graphite substrates.

Dwell time	Final temperature	Final pressure	Initial pressure
3 min	1850 °C	25 MPa	10 MPa

The sintering conditions used for the formation of the single protective layers are given in Table 8. It should be noted that to achieve better results and optimize processing variables, some single protective layers were applied to the M-2 sample at lower SPS temperatures and dwell times.

3. Results and discussion

3.1. Challenges of applying double protective layers

The protective layers studied in this section have been applied by SPS technology on the type SB-1 graphite substrates. Fig. 4 shows the optical microscopy images of the surface of the double protective layer of the Z-1 sample. Cracks and separations can be observed on the surface of the composite layer. Such defects are mainly caused by stresses during cooling rapid cooling of the sample due to the mismatch of the thermal expansion coefficients of the graphite substrate with the UHTC-based composite layers. Inadequate thickness of the intermediate layer can be mentioned as another reason for these defects.

Fig. 5 shows the macroscopic images of the surfaces of the Z-2, Z-3 and Z-4 samples. As it can be seen, the outer composite layers do not have a proper connection with the intermediate layers and the graphite substrates. This problem may be occurred owing to the following reasons:

-Mismatch between the thermal expansions coefficients of the composite layers and the graphite substrate.

-Inappropriate SPS conditions (temperature, dwell time and/or applied pressure).

-Insufficient thickness of the intermediate layer.

-Inappropriate chemical composition of the intermediate and/or the outer layers.

As seen in the macroscopic image of the surface of the T-1 sample (Fig. 6), despite the changes in the chemical composition of the outer layer (addition of Si) and the intermediate layer, the double protective layer is not properly bonded and it is separated from the graphite substrate. Optical microscopy images of the surface and the cross-section of the central part of the T-1 sample are shown in Fig. 7. The applied layers are peeled off at the edges of the sample, but the central area is relatively connected to the substrate. Therefore, the strategy of adding Si to the outer layer and increasing its amount in the intermediate layer did not have an interesting result.

Table 7. Chemical compositions of the single protective layers considered for the second methodology.

Sample code	Composition (vol%)				
	ZrB_2	SiC	Si	$MoSi_2$	WC
M-1	70	15	15	0	0
M-2	66.4	14.3	14.3	2.5	2.5
M-3	62.94	13.53	13.53	5	5

Fig. 8 shows a macroscopic image of the protective layer applied to the T-2 sample. Here, the thickness of the intermediate layer was decreased from 300 to 200 μm to reduce the effect of thickness on the mismatch in coefficients of thermal expansion of the applied layer with the graphite substrate. There are many cracks on the surface that separated the protective layers from the edges of the sample. Hence, reducing the thickness of the intermediate layer did not have a tangible effect on improving the bonding of the applied layer.

A macroscopic image of the protective layer applied to the T-3 sample is presented in Fig. 9. It should be noted that in this sample, the intermediate layer was eliminated from its design of experiment, but the outer layer contained Si additive. On one hand, there are many long and short cracks on the surface. On the other hand, non-uniformity on the surface of the applied composite layer is also visible, may be due to the surface melting.

In addition to the above-mentioned efforts, changes were made in the SPS process parameters, which can be listed as follows:

-Reducing the number of graphite foils used between the sample and the mold.

-Changing the electrical current and the maximum temperature.

-Changing the dwell time at maximum temperature.

-Holding at 1300 °C for 5 min.

-Applying maximum pressure at 1800 °C before reaching the final temperature.

Unfortunately, none of the new SPS conditions had a positive effect on the adhesion of the composite layer to the graphite substrate as the applied layers contained cracks and were separated from the substrate in some parts. Therefore, based on the observations in the first

Table 8. The SPS conditions for applying the UHTC-based layers on the type TC-90 graphite substrates.

Sample code	SPS conditions				
	Initial pressure	Final pressure	Final temperature	Dwell time at 1300 °C	Dwell time at final temperature
M-1	10 MPa	25 MPa	1950 °C	5 min	10 min
M-2	10 MPa	25 MPa	1950 °C	5 min	10 min
M-3	10 MPa	25 MPa	1950 °C	5 min	10 min
M-2(2)	10 MPa	25 MPa	1872 °C	5 min	10 min
M-2(3)	10 MPa	25 MPa	1840 °C	5 min	5 min

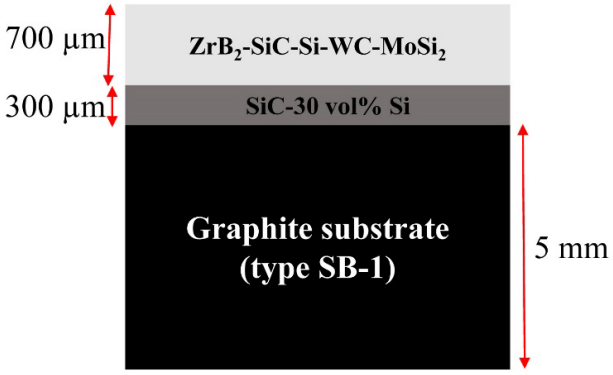

Fig. 2. Schematic of the arrangement of the double protective layers on the type SB-1 graphite substrates.

methodology, it seems that the changes in the chemical composition and the thickness of the applied layer, removal of the intermediate layer and changes in the SPS process conditions have not greatly improved the quality of the protective layer created on the type SB-1 graphite substrate. Therefore, due to the fact that several effective factors were investigated but no acceptable result was obtained, it is likely that there is a problem with the substrate material, actually with its thermal expansion coefficient.

3.2. Challenges of applying single protective layers

The single protective layers investigated in this section have been applied by the SPS route on the TC-90 graphite substrates. Fig. 10 shows the macroscopic images of the surfaces of the M-1, M-2 and M-3 samples. As it can be clearly seen, there is a kind of melting in the center of the composite layers. It seems that the temperature in the center of the samples was higher than the edges, which may be due to the high applied current and the electrical/thermal conductivity of $MoSi_2$ [49]. The presence of many cracks in the surrounding areas, the edges of the samples, indicates that the sintering process has not been completed and due to the low temperature in these areas, proper connections between the graphite substrates and the composite layers

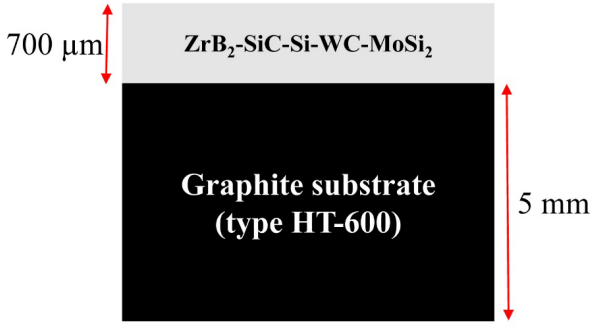

Fig. 3. Schematic of the arrangement of the single protective layers on the type TC-90 graphite substrates.

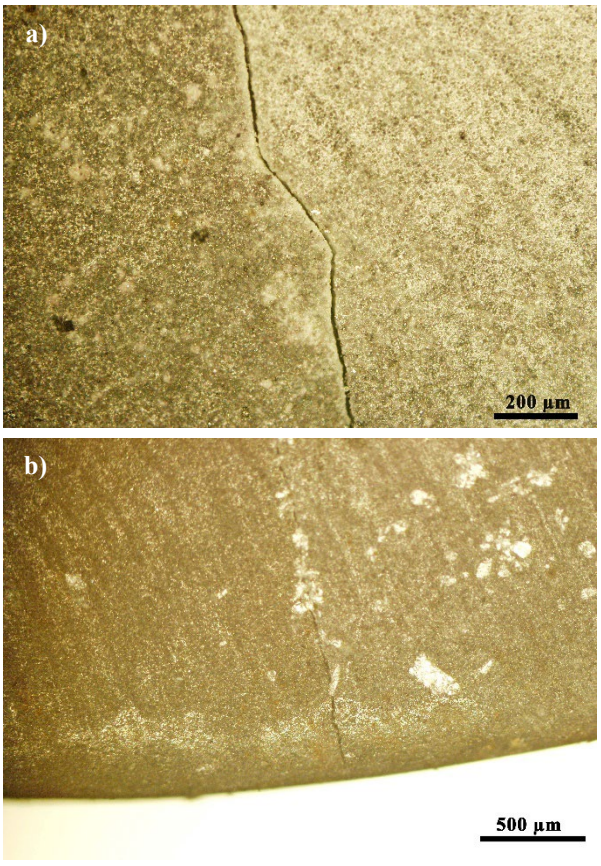

Fig. 4. Optical microscopy images of the surface of the double protective layer of the Z-1 sample.

have not been established. It appears that these cracks occurred during the samples cooling step, due to the mismatch of the thermal expansion coefficients between the substrates and the applied layers. Considering that the thermal expansion coefficients of ZrB_2, SiC, Si, WC, $MoSi_2$ and TC-90 graphite are 6.6×10^{-6} [47], 5×10^{-6} [47], 2.5×10^{-6} [50], 5.2×10^{-6} [51], 8.1×10^{-6} [52] and 5×10^{-6} K^{-1}, respectively, the mismatch between the applied protective layers with the graphite substrates may lead to cracking, separation or even delamination of the coating [46].

A comparison of the macroscopic images shown in Fig. 10 indicates that the M-3 sample includes more melting in the central zone than the M-2 sample, due to its more $MoSi_2$ content. It is found that unlike the M-2 sample that has short cracks, the M-3 sample has long and deep cracks that extend from the center to the edges of the sample. The presence of a thermal gradient between the center and surrounding areas can also be assumed, which causes stress and subsequently creates cracks. The optical microscopy images of the interface of melted/non-melted areas and the cross-section of the melted zone in the M-2 sample are shown in Fig. 11.

In order to solve the above-mentioned defects, which are probably due to the high temperature (high applied current) and the concentration of the current in the center of the samples, new composite layers were applied to the type TC-90 graphite substrates under milder SPS conditions (lower applied current and shorter dwell time). The

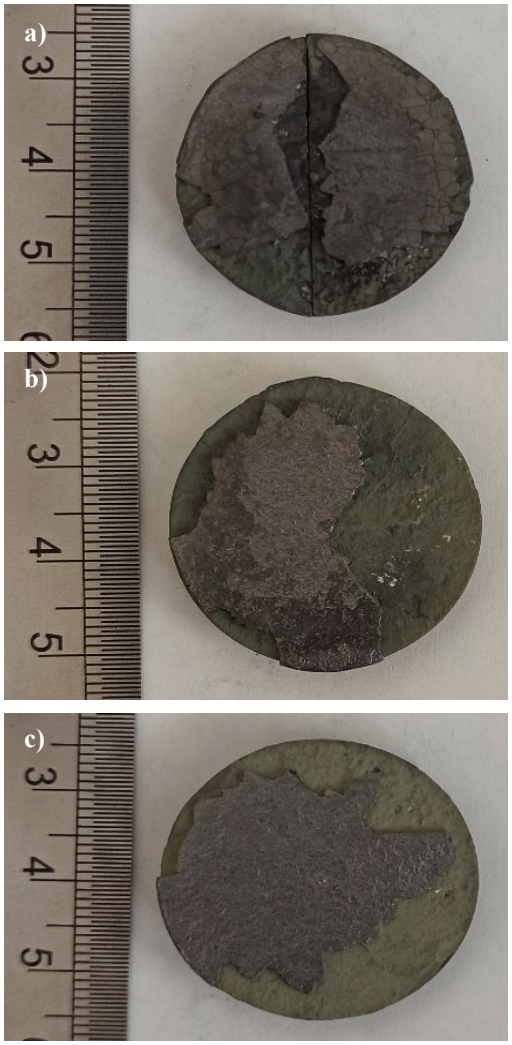

Fig. 5. Macroscopic images of the double protective layers of the a) Z-2, b) Z-3, and c) Z-4 samples.

macroscopic images of these new samples (M-2(2) and M-2(3)) are shown in Fig. 12. Compared to the observations of sample M-2 (Fig. 10b), the melting defects and the number of cracks are decreased

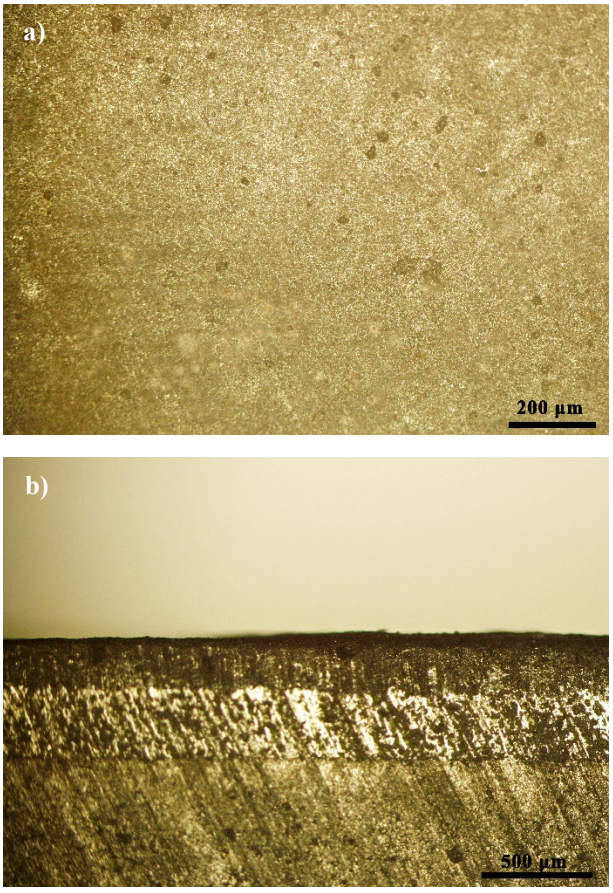

Fig. 7. Optical microscopy image of a) the surface and b) the cross-section of the central part of the T-1 sample.

by moderating the sintering conditions. Although the melting defect in the center of the applied layer can be eliminated by adjusting the SPS conditions, some cracks are still observed on the surface of the applied layers. However, the authors of this paper will continue to research in this field and if better results are obtained, we will publish them in the future.

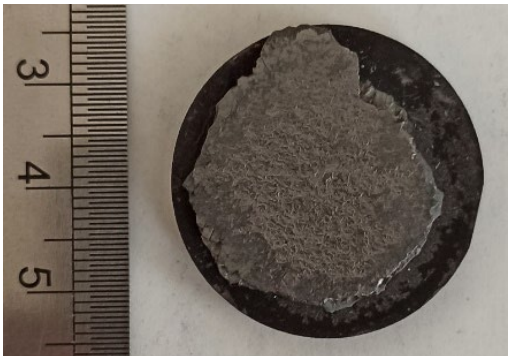

Fig. 6. Macroscopic image of the double protective layer of the T-1 sample.

Fig. 8. Macroscopic image of the double protective layer of the T-2 sample.

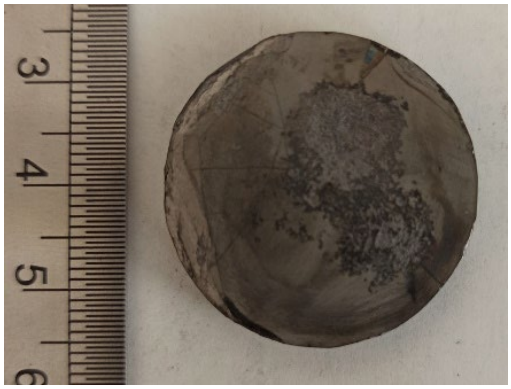

Fig. 9. Macroscopic image of the single protective layer of the T-3 sample.

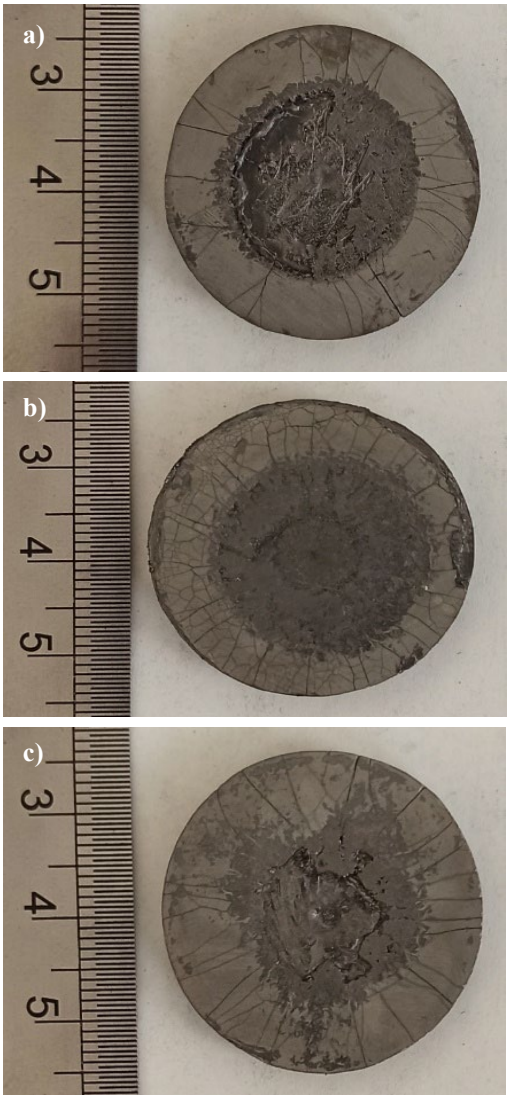

Fig. 10. Macroscopic images of the single protective layers of the a) M-1, b) M-2, and c) M-3 samples.

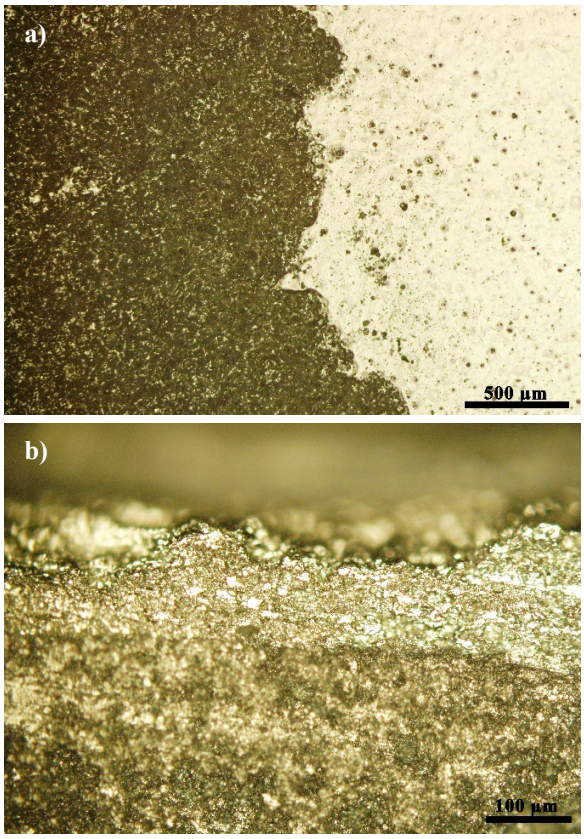

Fig. 11. Optical microscopy images of a) the interface of melted/non-melted areas and b) the cross-section of the melted zone in the M-2 sample.

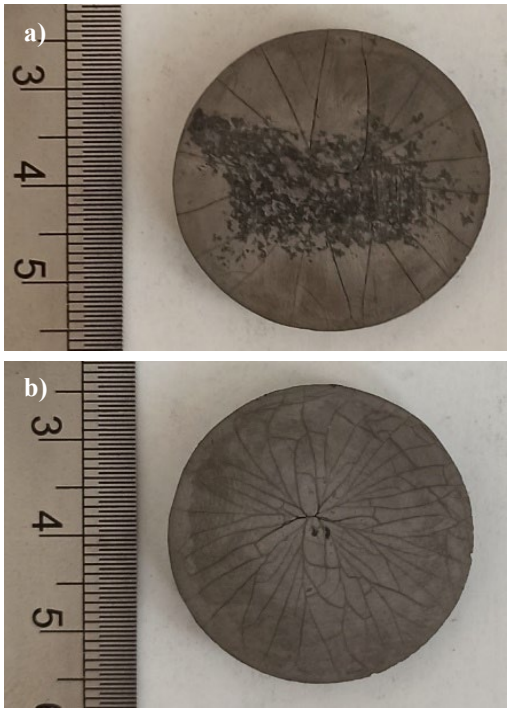

Fig. 12. Macroscopic images of the single protective layers of the a) M-2(2) and b) M-2 (3) samples.

4. Conclusions

In this study, challenges of applying protective UHTC-based composite layers on the graphite substrates using the SPS method were studied. Based on the observations, the layers applied on the graphite had many problems such as cracks, separation, weak adhesion, and melting. The results showed that several factors affect the connection of the protective composite layer to the graphite substrate. The most important factor was the mismatch between the thermal expansion coefficients of the graphite substrate and the applied composite layer.

CRediT authorship contribution statement

Mehran Jaberi Zamharir: Investigation, Project administration, Data curation, Formal Analysis, Writing – original draft.
Mohammad Zakeri: Formal Analysis, Resources, Funding acquisition, Supervision, Validation, Writing – review & editing.
Mansour Razavi: Funding acquisition, Supervision.

Data availability

The data underlying this article will be shared on reasonable request to the corresponding author.

Declaration of competing interest

The authors declare no competing interests.

Funding and acknowledgment

This article is derived from the PhD thesis of the first author, bearing tracking code 1464813 at the Iranian Research Institute for Information Science and Technology (IranDoc). The authors wish to extend their deepest gratitude to the Materials and Energy Research Center and all those who provided assistance in the completion of this thesis.

References

[1] Z. Dong, B. Sun, H. Zhu, G. Yuan, B. Li, et al., A review of aligned carbon nanotube arrays and carbon/carbon composites: fabrication, thermal conduction properties and applications in thermal management, New Carbon Mater. 36 (2021) 873–892. https://doi.org/10.1016/S1872-5805(21)60090-2.

[2] J.D. Webster, M.E. Westwood, F.H. Hayes, R.J. Day, R. Taylor, et al., Oxidation Protection Coatings for C/SiC based on Yttrium Silicate, J. Eur. Ceram. Soc. 18 (1998) 2345–2350. https://doi.org/10.1016/S0955-2219(98)00241-6.

[3] S.M. Gee, J.A. Little, Oxidation behaviour and protection of carbon/carbon composites, J. Mater. Sci. 26 (1991) 1093–1100. https://doi.org/10.1007/BF00576792.

[4] S. Chen, X. Qiu, B. Zhang, J. Xu, F. Zhong, et al., Advances in antioxidation coating materials for carbon/carbon composites, J. Alloys Compd. 886 (2021) 161143. https://doi.org/10.1016/j.jallcom.2021.161143.

[5] T. Cheng, Understanding the ultra-high-temperature mechanical behaviors of advanced two-dimensional carbon-carbon composites, Ceram. Int. 46 (2020) 21395–21401. https://doi.org/10.1016/j.ceramint.2020.05.237.

[6] J.H. Kim, A.Y. Jo, Y.J. Choi, K.B. Lee, J.S. Im, B.C. Bai, Improving the mechanical strength of carbon–carbon composites by oxidative stabilization, J. Mater. Res. Technol. 9 (2020) 16513–16521. https://doi.org/10.1016/j.jmrt.2020.11.064.

[7] J. Wang, X. Zhang, Z. Li, Y. Ma, L. Ma, Recent progress of biomass-derived carbon materials for supercapacitors, J. Power Sources. 451 (2020) 227794. https://doi.org/10.1016/j.jpowsour.2020.227794.

[8] E. Fitzer, L.M. Manocha, Carbon Reinforcements and Carbon/Carbon Composites, Springer Berlin Heidelberg, Berlin, Heidelberg. (1998). https://doi.org/10.1007/978-3-642-58745-0.

[9] B.D. Agarwal, L.J. Broutman, C.W. Bert, Analysis and Performance of Fiber Composites, J. Appl. Mech. 48 (1981) 213–213. https://doi.org/10.1115/1.3157582.

[10] D.E. Wittmer, M.Z. Temuri, Thermochemical Studies in Selected Metal-Carbon-Oxygen Systems, J. Am. Ceram. Soc. 74 (1991) 973–982. https://doi.org/10.1111/j.1151-2916.1991.tb04330.x.

[11]A. Tyagi, R.S. Walia, Q. Murtaza, S.M. Pandey, P.K. Tyagi, B. Bajaj, A critical review of diamond like carbon coating for wear resistance applications, Int. J. Refract. Met. Hard Mater. 78 (2019) 107–122. https://doi.org/10.1016/j.ijrmhm.2018.09.006.

[12] P. Wang, M. Tong, H. Wang, H. Li, Y. Jia, et al., Gradient HfB2-SiC multilayer oxidation resistant coating for C/C composites, Ceram. Int. 44 (2018) 20968–20973. https://doi.org/10.1016/j.ceramint.2018.08.104.

[13] R.V. Krishnarao, M.Z. Alam, D.K. Das, In-situ formation of SiC, ZrB2-SiC and ZrB2-SiC-B4C-YAG coatings for high temperature oxidation protection of C/C composites, Corros. Sci. 141 (2018) 72–80. https://doi.org/10.1016/j.corsci.2018.07.002.

[14] Q. Fu, P. Zhang, L. Zhuang, L. Zhou, J. Zhang, et al., Micro/nano multiscale reinforcing strategies toward extreme high-temperature applications: Take carbon/carbon composites and their coatings as the examples, J. Mater. Sci. Technol. 96 (2022) 31–68. https://doi.org/10.1016/j.jmst.2021.03.076.

[15] X. Jin, X. Fan, C. Lu, T. Wang, Advances in oxidation and ablation resistance of high and ultra-high temperature ceramics modified or coated carbon/carbon composites, J. Eur. Ceram. Soc. 38 (2018) 1–28. https://doi.org/10.1016/j.jeurceramsoc.2017.08.013.

[16] Y. Jiang, T. Liu, H. Ru, W. Wang, C. Zhang, X. Yue, Oxidation and ablation protection of double layer HfB2-SiC-Si/SiC-Si coating for graphite materials, J. Alloys Compd. 782 (2019) 761–771. https://doi.org/10.1016/j.jallcom.2018.12.256.

[17] S. Fan, X. Ma, Z. Li, J. Hu, Z. Xie, et al., Design and optimization of oxidation resistant coating for C/C aircraft brake materials, Ceram. Int. 44 (2018) 175–182. https://doi.org/10.1016/j.ceramint.2017.09.156.

[18] E. Wuchina, E. Opila, M. Opeka, B. Fahrenholtz, I. Talmy, UHTCs: Ultra-High Temperature Ceramic Materials for Extreme Environment Applications, Electrochem. Soc. Interface. 16 (2007) 30. https://doi.org/10.1149/2.F04074IF.

[19] B.R. Golla, A. Mukhopadhyay, B. Basu, S.K. Thimmappa, Review on ultra-high temperature boride ceramics, Prog. Mater. Sci. 111 (2020) 100651. https://doi.org/10.1016/j.pmatsci.2020.100651.

[20] Z. Balak, M. Zakeri, M. Rahimipour, E. Salahi, Taguchi design and hardness optimization of ZrB2-based composites reinforced with chopped carbon fiber and different additives and prepared by SPS, J. Alloys Compd. 639 (2015) 617–625. https://doi.org/10.1016/j.jallcom.2015.03.131.

[21] J.K. Sonber, T.S.R.C. Murthy, S. Majumdar, V. Kain, Processing of ZrB2- and HfB2-Based Ultra-High Temperature Ceramic Materials: A Review, Mater. Perf. Charact. 10 (2021) 89–121. https://doi.org/10.1520/MPC20200133.

[22] W.G. Fahrenholtz, G.E. Hilmas, I.G. Talmy, J.A. Zaykoski, Refractory Diborides of Zirconium and Hafnium, J. Am. Ceram. Soc. 90 (2007) 1347–1364. https://doi.org/10.1111/j.1551-2916.2007.01583.x.

[23] Z. Bahararjmand, M.A. Khalilzadeh, F. Saberi-Movahed, T.H. Lee, J. Wang, et al., Role of Si3N4 on microstructure and hardness of hot-pressed ZrB2−SiC composites, Synth. Sinter. 1 (2021) 34–40. https://doi.org/10.53063/synsint.2021.1113.

[24] E.L. Corral, R.E. Loehman, Ultra-High-Temperature Ceramic Coatings for Oxidation Protection of Carbon–Carbon Composites, J. Am. Ceram. Soc. 91 (2008) 1495–1502. https://doi.org/10.1111/j.1551-2916.2008.02331.x.
[25] P. Panjan, A. Drnovšek, P. Gselman, M. Čekada, M. Panjan, Review of Growth Defects in Thin Films Prepared by PVD Techniques, Coatings. 10 (2020) 447. https://doi.org/10.3390/coatings10050447.
[26] L. Tagliaferri, E. Berretti, A. Giaccherini, S.M. Martinuzzi, F. Bozza, et al., Aluminizing via Ionic Liquid Electrodeposition and Pack Cementation: A Comparative Study with Inconel 738 and a CoNiCrAlY, Coatings. 7 (2017) 83. https://doi.org/10.3390/coatings7060083.
[27] A. Zakeri, M.R. Masoumi Balashadehi, A. Sabour Rouh Aghdam, Development of hybrid electrodeposition/slurry diffusion aluminide coatings on Ni-based superalloy with enhanced hot corrosion resistance, J. Compos. Compd. 2 (2021) 1–8. https://doi.org/10.52547/jcc.3.1.1.
[28] J. Dong, Y. Sun, F. He, H. Huang, J. Zhen, Effects of substrate surface roughness and aluminizing agent composition on the aluminide coatings by low-temperature pack cementation, Mater. Res. Express. 6 (2018) 036409. https://doi.org/10.1088/2053-1591/aaf586.
[29] S. Karimi, S.M. Arab, S.R. Hosseini Zeidabadi, S. Javadpour, Tribological behavior and mechanical properties of friction stir processed HDPE/Fe-Fe3O4 composites, Synth. Sinter. 1 (2021). https://doi.org/10.53063/synsint.2021.1350.
[30] M. Abdolahpour Salari, G. Merhan Muğlu, M. Rezaei, M. Saravana Kumar, H. Pulikkalparambil, S. Siengchin, In-situ synthesis of TiN and TiB2 compounds during reactive spark plasma sintering of BN–Ti composites, Synth. Sinter. 1 (2021) 48–53. https://doi.org/10.53063/synsint.2021.119.
[31] M. Shirani, M. Rahimipour, M. Zakeri, S. Safi, T. Ebadzadeh, ZrB2-SiC-WC coating with SiC diffusion bond coat on graphite by spark plasma sintering process, Ceram. Int. 43 (2017) 14517–14520. https://doi.org/10.1016/j.ceramint.2017.07.123.
[32] K.-T. Wang, L.-Y. Cao, J.-F. Huang, J. Fei, A mullite/SiC oxidation protective coating for carbon/carbon composites, J. Eur. Ceram. Soc. 33 (2013) 191–198. https://doi.org/10.1016/j.jeurceramsoc.2012.08.009.
[33] S.A.A. Shalmani, M. Sobhani, O. Mirzaee, M. Zakeri, Ablation resistance of graphite coated by spark plasma sintered ZrB2–SiC based composites, Bol. Soc. Esp. Ceram. 61 (2021) 604–610. https://doi.org/10.1016/j.bsecv.2021.05.004.
[34] Y. Miao, X. Wang, Y. Cheng, Carbon nanotube/titanium carbide sol-gel coated zirconium diboride composites prepared by spark plasma sintering, Ceram. Int. 44 (2018) 19262–19267. https://doi.org/10.1016/j.ceramint.2018.07.151.
[35] S.A. Akbarpour Shalmani, M. Sobhani, O. Mirzaee, M. Zakeri, Effect of HfB2 and WC additives on the ablation resistance of ZrB2–SiC composite coating manufactured by SPS, Ceram. Int. 46 (2020) 25106–25112. https://doi.org/10.1016/j.ceramint.2020.06.297.
[36] M. Ghassemi Kakroudi, M. Dehghanzadeh Alvari, M. Shahedi Asl, N. Pourmohammadie Vafa, T. Rabizadeh, Hot pressing and oxidation behavior of ZrB2–SiC–TaC composites, Ceram. Int. 46 (2020) 3725–3730. https://doi.org/10.1016/j.ceramint.2019.10.093.
[37] S. Haghgooye Shafagh, S. Jafargholinejad, S. Javadian, Beneficial effect of low BN additive on densification and mechanical properties of hot-pressed ZrB2–SiC composites, Synth. Sinter. 1 (2021) 69–75. https://doi.org/10.53063/synsint.2021.1224.
[38] F. Sadegh Moghanlou, M. Vajdi, H. Jafarzadeh, Z. Ahmadi, A. Motallebzadeh, et al., Spark plasma sinterability and thermal diffusivity of TiN ceramics with graphene additive, Ceram. Int. 47 (2021) 10057–10062. https://doi.org/10.1016/j.ceramint.2020.12.152.
[39] L. He, Y. Sun, Q. Meng, B. Liu, J. Wu, X. Zhang, Enhanced oxidation properties of ZrB2–SiC composite with short carbon fibers at 1600 °C, Ceram. Int. 47 (2021) 15483–15490. https://doi.org/10.1016/j.ceramint.2021.02.114.
[40] M. Dehghanzadeh Alvari, M. Ghassemi Kakroudi, B. Salahimehr, R. Alaghmandfard, M. Shahedi Asl, M. Mohammadi, Microstructure, mechanical properties, and oxidation behavior of hot-pressed ZrB2–SiC–B4C composites, Ceram. Int. 47 (2021) 9627–9634. https://doi.org/10.1016/j.ceramint.2020.12.101.
[41] I. FarahBakhsh, R. Antiochia, H.W. Jang, Pressureless sinterability study of ZrB2–SiC composites containing hexagonal BN and phenolic resin additives, Synth. Sinter. 1 (2021) 99–104. https://doi.org/10.53063/synsint.2021.1231.
[42] S.M. Arab, M. Shahedi Asl, M. Ghassemi Kakroudi, B. Salahimehr, K. Mahmoodipour, On the oxidation behavior of ZrB 2 –SiC–VC composites, Int. J. Appl. Ceram. Technol. 18 (2021) 2306–2313. https://doi.org/10.1111/ijac.13858.
[43] L. Silvestroni, C. Melandri, V. Venkatachalam, J. Binner, D. Sciti, Merging toughness and oxidation resistance in a light ZrB2 composite, Mater. Des. 183 (2019) 108078. https://doi.org/10.1016/j.matdes.2019.108078.
[44] W.G. Fahrenholtz, Thermodynamic Analysis of ZrB2-SiC Oxidation: Formation of a SiC-Depleted Region, J. Am. Ceram. Soc. 90 (2007) 143–148. https://doi.org/10.1111/j.1551-2916.2006.01329.x.
[45] S. Torabi, Z. Valefi, N. Ehsani, The effect of the SiC content on the high duration erosion behavior of SiC/ZrB2– SiC/ZrB2 functionally gradient coating produced by shielding shrouded plasma spray method, Ceram. Int. 48 (2022) 1699–1714. https://doi.org/10.1016/j.ceramint.2021.09.249.
[46] Y.-J. Wang, H.-J. Li, Q.-G. Fu, H. Wu, D.-J. Yao, B.-B. Wei, Ablative property of HfC-based multilayer coating for C/C composites under oxy-acetylene torch, Appl. Surf. Sci. 257 (2011) 4760–4763. https://doi.org/10.1016/j.apsusc.2010.11.020.
[47] X. Zou, Q. Fu, L. Liu, H. Li, Y. Wang, et al., ZrB2–SiC coating to protect carbon/carbon composites against ablation, Surf. Coat. Technol. 226 (2013) 17–21. https://doi.org/10.1016/j.surfcoat.2013.03.027.
[48] X. Yao, H. Li, Y. Zhang, H. Wu, X. Qiang, A SiC–Si–ZrB2 multiphase oxidation protective ceramic coating for SiC-coated carbon/carbon composites, Ceram. Int. 38 (2012) 2095–2100. https://doi.org/10.1016/j.ceramint.2011.10.047.
[49] Q. Fu, Y. Shan, C. Cao, H. Li, K. Li, Oxidation and erosion resistant property of SiC/Si–Mo–Cr/MoSi2 multi-layer coated C/C composites, Ceram. Int. 41 (2015) 4101–4107. https://doi.org/10.1016/j.ceramint.2014.11.105.
[50] T. Feng, H.-J. Li, Q.-G. Fu, X.-T. Shen, H. Wu, Microstructure and oxidation of multi-layer MoSi2–CrSi2–Si coatings for SiC coated carbon/carbon composites, Corros. Sci. 52 (2010) 3011–3017. https://doi.org/10.1016/j.corsci.2010.05.020.
[51] C.-S. Kim, T.R. Massa, G.S. Rohrer, Modeling the relationship between microstructural features and the strength of WC–Co composites, Int. J. Refract. Met. Hard Mater. 24 (2006) 89–100. https://doi.org/10.1016/j.ijrmhm.2005.04.011.
[52] T. Li, H. Li, X. Shi, Effect of LaB6 on the thermal shock property of MoSi2-SiC coating for carbon/carbon composites, Appl. Surf. Sci. 264 (2013) 88–93. https://doi.org/10.1016/j.apsusc.2012.09.124.